Cell adhesion to fibrillin-1: identification of an Arg-Gly-Asp-dependent synergy region and a heparin-binding site that regulates focal adhesion formation

Daniel V. Bax[1,2], Yashithra Mahalingam[3], Stuart Cain[2], Kieran Mellody[2], Lyle Freeman[2], Kerri Younger[2], C. Adrian Shuttleworth[2], Martin J. Humphries[2], John R. Couchman[3] and Cay M. Kielty[1,2,*]

[1]UK Centre for Tissue Engineering and [2]Wellcome Trust Centre for Cell-Matrix Research, Faculty of Life Sciences, University of Manchester, Manchester, M13 9PT, UK
[3]Faculty of Medicine, Imperial College London, Exhibition Road, London, SW7 2AZ, UK
*Author for correspondence (e-mail: cay.kielty@manchester.ac.uk)

Accepted 5 February 2007
Journal of Cell Science 120, 1383-1392 Published by The Company of Biologists 2007
doi:10.1242/jcs.003954

Summary

We have defined the molecular basis of cell adhesion to fibrillin-1, the major structural component of extracellular microfibrils that are associated with elastic fibres. Using human dermal fibroblasts, and recombinant domain swap fragments containing the Arg-Gly-Asp motif, we have demonstrated a requirement for upstream domains for integrin-$\alpha_5\beta_1$-mediated cell adhesion and migration. An adjacent heparin-binding site, which supports focal adhesion formation, was mapped to the fibrillin-1 TB5 motif. Site-directed mutagenesis revealed two arginine residues that are crucial for heparin binding, and confirmed their role in focal adhesion formation. These integrin and syndecan adhesion motifs juxtaposed on fibrillin-1 are evolutionarily conserved and reminiscent of similar functional elements on fibronectin, highlighting their crucial functional importance.

Supplementary material available online at
http://jcs.biologists.org/cgi/content/full/120/8/1383/DC1

Key words: Fibrillin-1, Cell adhesion, Integrins, Heparin, Syndecan-4, Fibronectin

Introduction

Fibrillin-1 is a large extracellular matrix glycoprotein and the major constituent of fibrillin-rich microfibrils (Kielty et al., 2005; Kielty, 2006). It contains 47 epidermal growth factor (EGF) domains, of which 43 are calcium binding (cbEGF)-like domains, and 7 eight-cysteine-containing TB motifs (Pereira et al., 1993) (Fig. 1). It has a single Arg-Gly-Asp (RGD) cell adhesion motif within the fourth TB repeat (TB4), which is surrounded by polar, charged amino acids and likely to be solvent exposed. By analogy with the high-resolution structures of other TB motifs (Yuan et al., 1997; Lack et al., 2003), the RGD motif is probably exposed on the end of a finger-like projection that is stabilised by two cysteine residues. Molecular modelling of TB4 and flanking domains indicates that the RGD loop may be highly mobile (Lee et al., 2004). The TB4 RGD motif is conserved in fibrillin-2 (Zhang et al., 1994).

Previous studies demonstrate that cell adhesion to fibrillin-1 and fibrillin-2 involves the RGD motif on TB4. Using recombinant fibrillin-1 fragments expressed in a mammalian system and purified integrins, it was shown that integrin αvβ3 was a fibrillin receptor (Pfaff et al., 1996). Fetal bovine chondrocytes stimulated by antibody activation bind to purified bovine fibrillin through α5β1 integrin (Sakamoto et al., 1996). We have shown that integrins αvβ3 and α5β1 can both bind to recombinant fibrillin-1 fragments expressed in a mammalian system, in a cell-specific manner (Bax et al., 2003). Studies using bacterially expressed constructs that were refolded using a redox shuffling system, which encompassed cbEGF22-TB4, TB4-cbEGF23 and cbEGF22-TB4-cbEGF23, show that the presence of a single cbEGF domain immediately N-terminal to TB4 influences cell attachment through integrin αvβ3 (Lee et al., 2004), but that only TB4 is required for keratinocyte adhesion through αvβ6 integrin (Jovanović et al., 2007).

Fibrillin-1 is a major heparin-binding molecule. Heparin-binding regions were identified on fibrillin-1 and a role for heparin in microfibril assembly was demonstrated (Tiedemann et al., 2001; Ritty et al., 2003). We showed that there are four high-affinity heparin-binding sites on fibrillin-1, defined the binding kinetics and identified two potential heparan sulphate binding sites within the third site (TB5-cbEGF 25; residues 1689-2055) by theoretical docking analysis (Cain et al., 2005). One of these heparin-binding sites occurs within a two-domain region close to TB4 (Fig. 1). The source of the heparin that binds fibrillin-1 remains unknown. Although fibrillin-1 binds perlecan, a basement membrane heparan sulphate proteoglycan, this is a protein-protein interaction (Tiedemann et al., 2005). It is possible that fibrillin-1 interacts with heparan sulphate proteoglycan cell surface receptors, which include syndecans (Alexopoulou et al., 2007). Co-engagement of α5β1 integrin and syndecan-4 by the adhesive glycoprotein fibronectin stimulates spreading and focal adhesion formation (Woods et al., 2000; Couchman, 2003; Humphries et al., 2005; Dovas et al., 2006).

In this study, we have defined a central region of fibrillin-1 in which cell adhesion, spreading and focal adhesion formation are profoundly modulated by specific domains upstream and

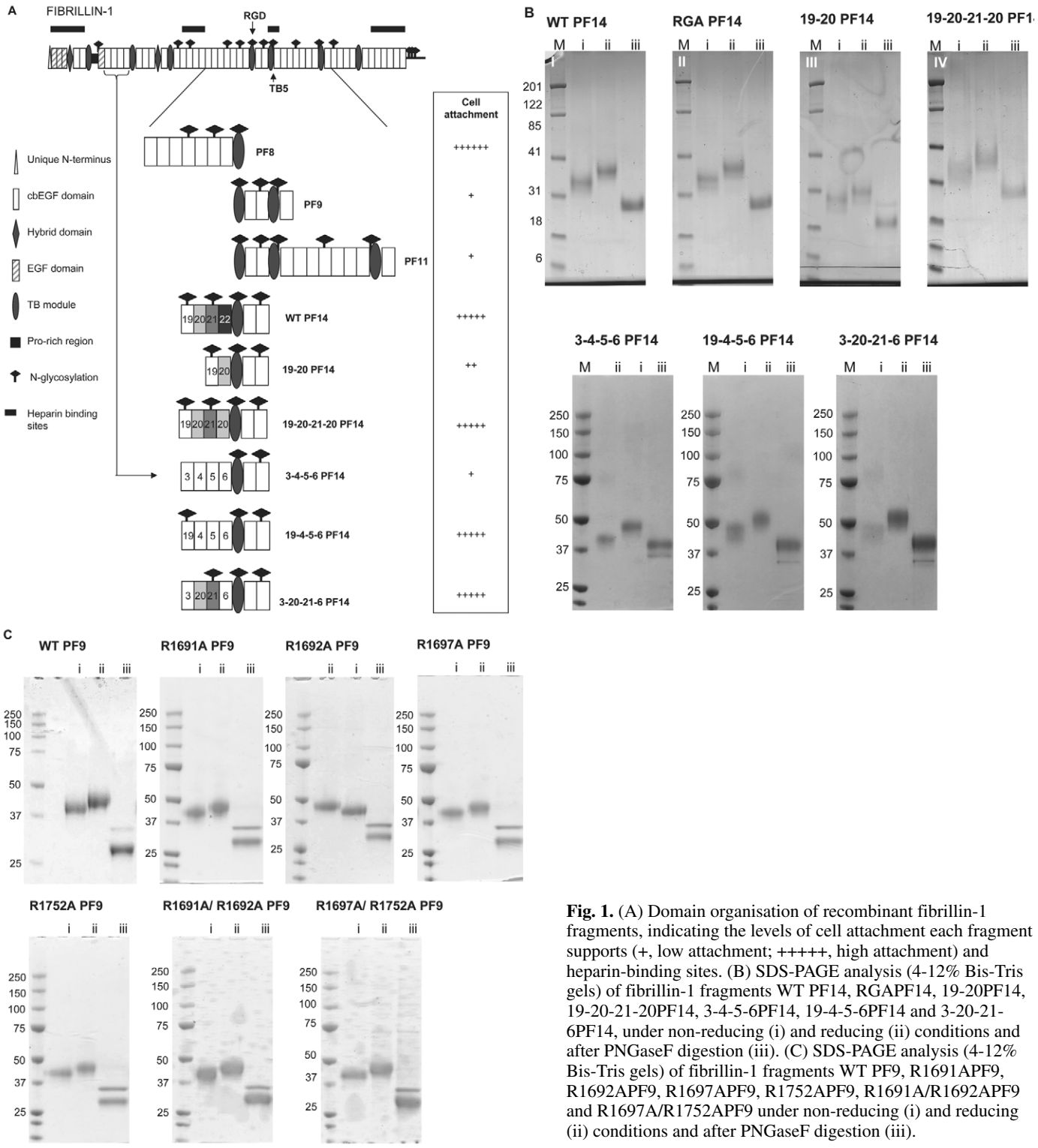

Fig. 1. (A) Domain organisation of recombinant fibrillin-1 fragments, indicating the levels of cell attachment each fragment supports (+, low attachment; +++++, high attachment) and heparin-binding sites. (B) SDS-PAGE analysis (4-12% Bis-Tris gels) of fibrillin-1 fragments WT PF14, RGAPF14, 19-20PF14, 19-20-21-20PF14, 3-4-5-6PF14, 19-4-5-6PF14 and 3-20-21-6PF14, under non-reducing (i) and reducing (ii) conditions and after PNGaseF digestion (iii). (C) SDS-PAGE analysis (4-12% Bis-Tris gels) of fibrillin-1 fragments WT PF9, R1691APF9, R1692APF9, R1697APF9, R1752APF9, R1691A/R1692APF9 and R1697A/R1752APF9 under non-reducing (i) and reducing (ii) conditions and after PNGaseF digestion (iii).

downstream of the RGD motif. An upstream cbEGF domain array regulates RGD-dependent adhesion. A downstream heparan sulphate binding site has been mapped that induces focal adhesions. The presence of functionally similar cell adhesion elements on fibrillin-1 and the structurally unrelated adhesive glycoprotein, fibronectin, highlight their critical evolutionary importance in cell-matrix biology.

Results

We have previously shown that fibrillin-1 interacts with cells through integrins $\alpha5\beta1$ and $\alpha v\beta3$, in an RGD-dependent manner (Bax et al., 2003). Cell binding to fibronectin through integrin $\alpha5\beta1$ requires synergy sites, in addition to the RGD motif, for full cell binding (Redick et al., 2000). For full cytoskeletal organisation with focal adhesions, the ligation of

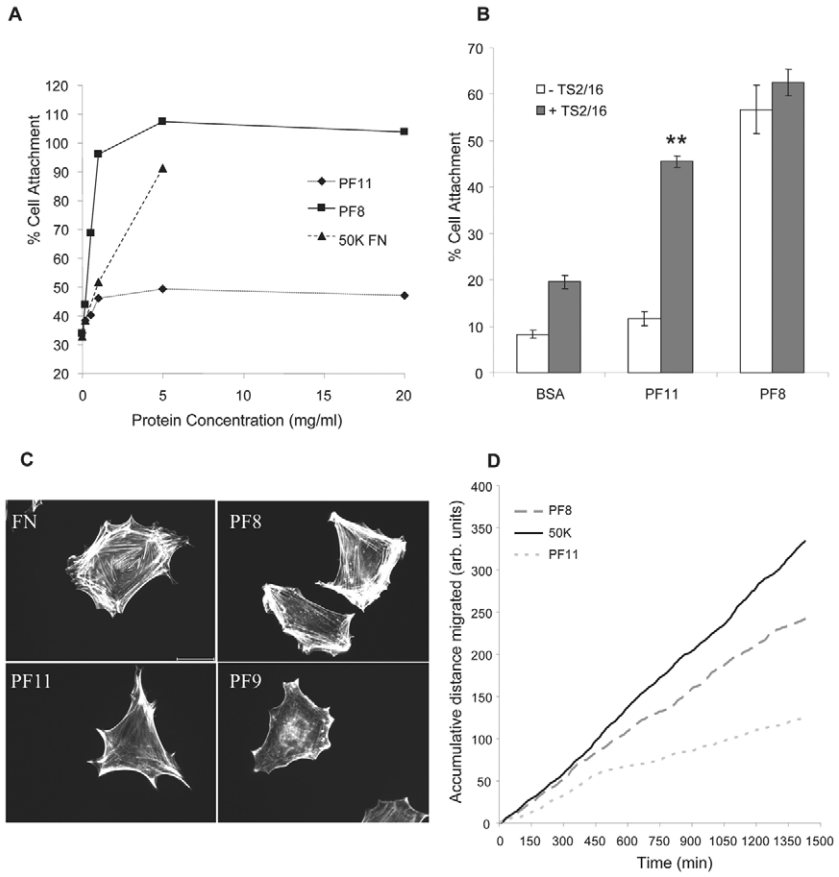

Fig. 2. (A) Dose-dependent HDF attachment to fibrillin-1 fragments PF8 (squares), PF11 (diamonds) and the central cell binding region of fibronectin (50K-FN) (triangles). (B) HDF attachment to 10 μg/ml PF11, PF8 or BSA-blocked plastic in the presence (shaded) or absence (open) of the β1-integrin-activating antibody TS2/16. Data were statistically analysed using unpaired Student's *t*-tests (GraphPad Prism 2.0). Error bars represent the s.d. of the three experiments. (C) Fluorescence images of actin filaments in phalloidin-stained spread fibroblasts on fibronectin, PF11, PF8 and PF9. There were no spread cells in the BSA control (not shown). (D) Cumulative distance travelled by cells adherent to 50K-FN (solid line), PF8 (long dashed line) or PF11 (short dashed line), as measured by time lapse microscopy. Bar, 50 μm.

cell surface syndecan-4 via heparan sulphate binding regions is also required (Woods et al., 2000). As fibrillin-1 contains heparan sulphate binding sites (Cain et al., 2005) as well as the ability to bind to cells through integrin α5β1 (Bax et al., 2003), we used fibroblasts to ask two questions. (1) Does RGD-dependent cell adhesion to fibrillin-1 require a synergy site(s)? (2) Does engagement of a fibrillin-1 heparan sulphate binding site promote cytoskeletal assembly?

Fibrillin-1 RGD-dependent cell adhesion requires a synergy site for full cell binding activity

Effects of cbEGF-like domains upstream of TB4 on fibroblast adhesion, spreading, cytoskeletal organisation and migration

Our previous study showed that the TB4 motif and downstream domains (fragments PF9 and PF11) support integrin α5β1- and αvβ3-mediated cell adhesion (Bax et al., 2003), whereas upstream cbEGF 22 has been shown to influence cell adhesion through integrin αvβ3 (Lee et al., 2004). Here, we investigated whether the presence of cbEGF-like domains N-terminal to TB4 influence primary human dermal fibroblast (HDF) adhesion through integrins α5β1 and/or αvβ3.

Initially, we compared two overlapping fibrillin-1 fragments – PF8, which contains TB4 plus seven upstream domains and PF11, which contains TB4 plus twelve downstream domains (for domain structures, see Fig. 1A) – to determine whether N- or C-terminal cbEGF-like domains influence cell adhesion (Fig. 2A). PF8 supported strong cell adhesion, which was greater than that supported by the central cell binding fragment of fibronectin (50K-FN). By contrast, PF11 supported much lower cell adhesion than either PF8 or 50K-FN. The β1-activating mAb TS2/16 significantly enhanced adhesion to PF11 but not to PF8 (Fig. 2B). Cells on PF8 showed a well-spread morphology that was similar to cells plated on plasma fibronectin (Fig. 2C). However, cells plated on PF9 and PF11 were generally smaller and much less well spread.

When HDF migration on PF8, PF11 or fibronectin was monitored in real time, the accumulative distance migrated was greatest for cells on fibronectin, then on PF8 and then on PF11 (Fig. 2D). These data show that PF8 supports much stronger cell adhesion, cell spreading and migration than PF11. Thus, the cbEGF-like domains upstream of TB4 enhance cell binding and signalling.

Contributions of specific cbEGF-like domains N terminal to TB4 in modulating cell adhesion and spreading

To determine which upstream cbEGF-like domains enhance cell adhesion and spreading on fibrillin-1, removal and addition of upstream domains was undertaken. Owing to problematic restriction sites in PF8, an additional fragment, PF14, was generated which contained only four upstream cbEGF-like domains (see Fig. 1). This fragment was amenable to site-directed mutagenesis for domain swap experiments, and also supported strong cell adhesion, although slightly lower than that seen with PF8 (Fig. 3A). All swapped domains preserved the correct domain boundaries and had similar secondary structures (Table 1).

As cbEGF 22 has been shown to influence αvβ3-mediated cell adhesion (Lee et al., 2004), we generated two constructs

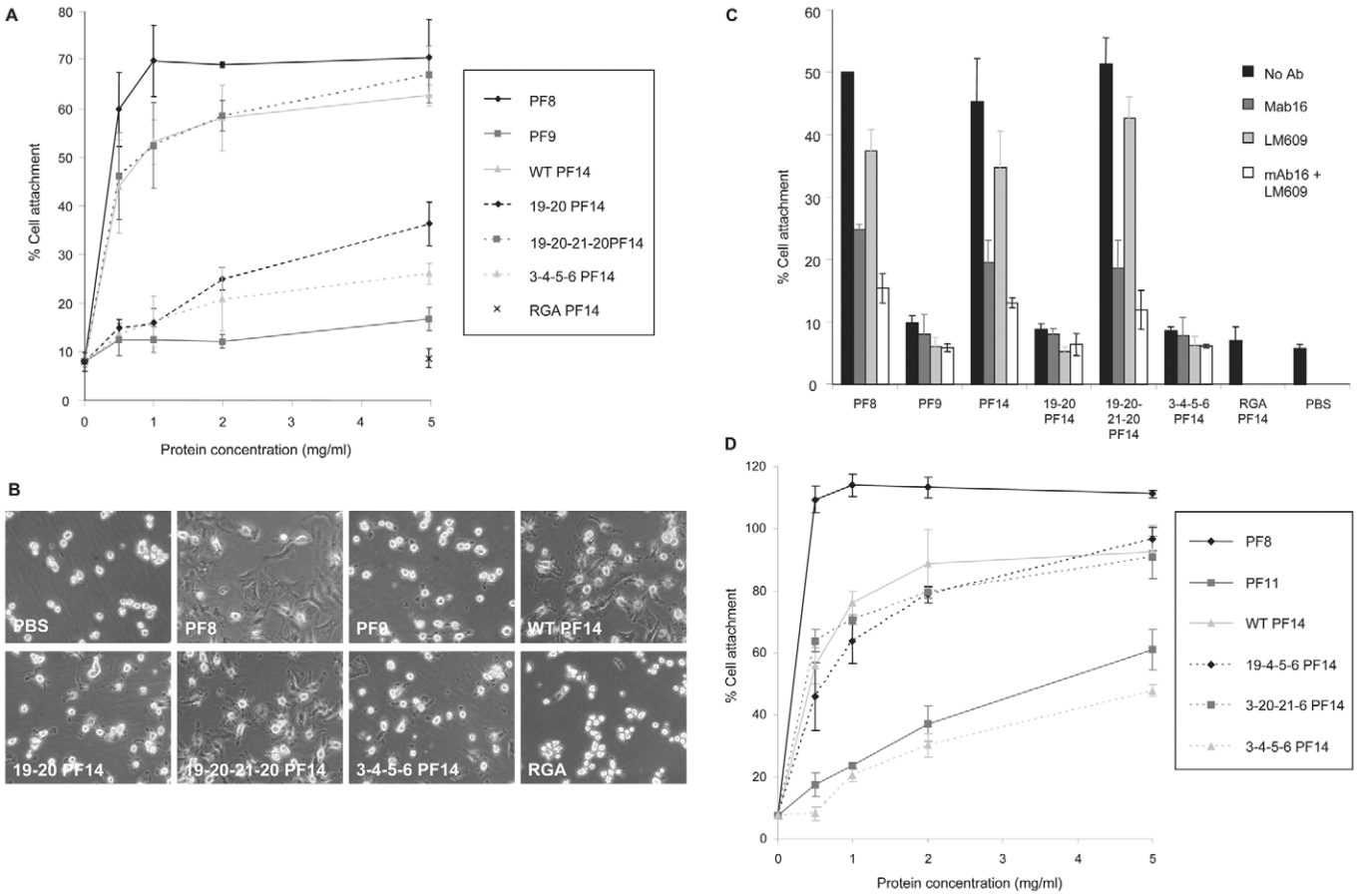

Fig. 3. (A) HDF attachment to fibrillin-1 fragments PF8, PF9, WT PF14 and PF14 mutants 19-20PF14, 19-20-21-20PF14, 3-4-5-6PF14 and RGA PF14. (B) Phase-contrast photographs of HDFs spreading onto PF8, PF9, WT PF14, 19-20PF14, 19-20-21-20PF14, 3-4-5-6PF14, RGA PF14 and control wells (PBS). (C) Anti-integrin antibody inhibition of HDF attachment to PF8, PF9, WT PF14, 19-20PF14, 19-20-21-20PF14, 3-4-5-6PF14, RGA PF14 and control wells (PBS). (D) HDF attachment to fibrillin-1 fragments PF8, PF11, WT PF14 and the PF14 mutants 19-4-5-6PF14, 3-20-21-6PF14 and 3-4-5-6PF14.

in which cbEGF 21 and 22 were removed (19-20PF14), and in which cbEGF 22 was replaced with cbEGF 20 (19-20-21-20PF14) (see Fig. 1B). Fragment 19-20-21-20PF14 showed similar cell adhesion to WT PF14, so cbEGF 20 can substitute for cbEGF 22 without loss of adhesion (Fig. 3A). However, 19-20PF14 showed a lower level of cell attachment than WT PF14, indicating that all four upstream domains are required for the strongest attachment (Fig. 3A). A further mutant was constructed in which cbEGF 19-22 were replaced with cbEGF 3-6 (3-4-5-6PF14) to determine whether a specific upstream sequence was responsible for increased cell binding. HDF attachment to 3-4-5-6PF14 was much lower than WT PF14, but comparable with PF9, which contains no domains upstream of TB4 (Bax et al., 2003) (Fig. 3A). Interestingly, 3-4-5-6PF14 had a greater reduction in cell attachment than 19-20PF14, indicating that 19-20PF14 does enhance cell binding although to a much lower level than when four upstream cbEGF-like domains are present. An RGD-to-RGA PF14 (RGAPF14) mutant showed only baseline levels of attachment, confirming that the increased cell binding caused by the presence of upstream cbEGF-like domains was RGD dependent (Fig. 3A).

HDF spreading levels on the wild-type and mutant PF14 fragments correlated with HDF adhesion levels on these fragments (Fig. 3B). WT PF14, 19-20-21-20PF14 and PF8 all showed high levels of cell spreading. However, 19-20PF14 supported less cell spreading, whereas 3-4-5-6PF14 and PF9 supported only very low levels of cell spreading. The RGAPF14 mutant supported no cell spreading. Thus, HDFs require four upstream cbEGF-like domains for strong cell adhesion and migration. However, cbEGF 22 does not contain any specific synergy sequences, as it can be substituted without loss of adhesion. To refine and confirm the requirement for upstream cbEGF 19, 20 and/or 21 for increased cell binding, knock-in mutants (see Fig. 1) were examined (Fig. 3D), based on the 3-4-5-6PF14 fragment that had very weak adhesion and spreading (see Fig. 3A,B). cbEGF 19 was knocked into 3-4-5-6PF14, in its appropriate position, in place of cbEGF 3 (19-4-5-6PF14) and cbEGF 20 and 21 were together knocked into 3-4-5-6PF14 in place of cbEGF 4 and 5, respectively (3-20-21-6PF14). As substitution of cbEGF 22 with 20 had no effect on cell binding (see Fig. 3A), it was excluded from the knock-in experiment. Knock-in 19-4-5-6PF14 and 3-20-21-6PF14 fragments both rescued 3-6PF14-mediated cell adhesion, to the level of wild-type PF14 (Fig. 3D). Thus, the specific cbEGF-like domain array 19-21 upstream of cbEGF 22 is needed for strong cell adhesion.

Integrins mediate fibroblast attachment to TB4-containing fragments

Previously we showed that fibrillin-1 fragments containing cbEGF-like domains downstream of TB4 bound to cells through both integrins α5β1 and/or αVβ3 (Bax et al., 2003). Therefore, to evaluate whether the integrin-binding profile was influenced by the presence of upstream cbEGF-like domains, HDF attachment assays were performed in the presence or absence of integrin function-blocking monoclonal antibodies mAb16 (anti α5) or LM609 (anti αVβ3) (Fig. 3C). Cell attachment to PF8, PF14 and 19-20-21-20PF14 was strongly inhibited by mAb16, and much less by LM609. By contrast, cell attachment to PF9, 19-20PF14 and 3-4-5-6PF-14, which was much lower than to PF8, PF14 and 19-20-21-20PF14, was inhibited more by LM609 than by mAb16.

Thus, swapping cbEGF-like domains 19-21 altered integrin engagement. HDF attached to PF8, PF14 and 19-20-21-20PF14 mainly through integrin α5β1, but with some involvement of αVβ3, whereas HDF attachment to PF9, 19-20PF14 and 3-4-5-6PF14 was very weak and more through αVβ3 than α5β1. Thus, four upstream cbEGF-like domains are necessary for enhanced integrin binding activity and cbEGF-like domains 19 or 20-21 are specifically required for more efficient cell adhesion through integrin α5β1.

Engagement of a fibrillin-1 heparan sulphate binding promotes cytoskeletal assembly

Cytoskeletal assembly on fibronectin requires integrin α5β1 engagement through its RGD motif, an upstream PHSRN synergy site (Redick et al., 2000) and also binding to syndecan-4 through a downstream heparan sulphate binding site (Woods et al., 2000). We have established that HDF attachment to fibrillin-1 fragments PF8 and PF14 occurs mainly through α5β1, which requires the presence of specific upstream domains and the RGD motif. As previously described (Cain et al., 2005), heparin interacts strongly with the overlapping fibrillin-1 fragments, PF9, PF10 and PF11, which allowed localisation of the site to TB5 and the following cbEGF-like domain 25 (see Fig. 1A). We therefore investigated whether this heparin-binding site can engage cell surface heparan sulphate, and thereby induce focal adhesion and stress fibre formation.

Overlapping fragments PF9 and PF10 stimulate focal adhesion and stress fiber formation in fibroblasts plated on PF8

For these studies, we used rat embryonic fibroblasts (REFs) and mouse embryonic fibroblasts (MEFs), since previous studies that demonstrate the requirement for heparan sulphate binding for the assembly of a robust cytoskeleton used these cells (Humphries et al., 2005; Dovas et al., 2006). Initially, REFs were used to investigate cytoskeletal morphology when plated on PF8, which has the RGD motif and upstream domains, to ensure strong α5β1-mediated adhesion, in the presence or absence of fibrillin-1 heparan sulphate binding fragments (Fig. 4). Cells on fibronectin were controls. Adherence to PF8 resulted in the formation of few vinculin-containing focal adhesions, in contrast to cells on fibronectin, which contained numerous focal adhesions. However, vinculin-containing focal adhesion assembly was markedly increased by the addition of soluble fibrillin-1 fragment PF10.

To confirm these results, actin cytoskeletal assembly and focal adhesion formation in MEFs adherent to PF8 was induced with the addition of PF9, PF10 or PF11, all of which contain the same heparan sulphate-binding site but in a different fragment context (Fig. 5A). Furthermore, PF9 and PF10 could also stimulate cytoskeletal assembly of REFs adhering to a fragment containing the fibronectin central cell-binding region (110FN) (Fig. 6A), in a manner similar to the heparan sulphate binding region of fibronectin (HepII) that is known to activate syndecan-4 (Woods et al., 2000). A PF9 RGD-to-RDG mutant had a similar stimulatory effect to WT PF9, with assembly of stress fibres and focal adhesions (Fig. 6A), so this effect is not influenced by the PF9 RGD motif. Thus, all three fibrillin-1 fragments that contain the heparin-binding site induce focal adhesions on the α5β1-integrin-ligating fragments PF8 or 110FN. These data show that heparan sulphate engagement is a likely mechanism for PF9, PF10 or PF11 stimulation of cytoskeletal assembly.

Mapping of the heparan sulphate binding site in PF9

Our previously reported 3D model for the docking of a heparin pentasaccharide to TB5-cbEGF-like domain 25 had predicted two potential binding sites within TB5 (Cain et al., 2005). To confirm that PF9 stimulation of cytoskeletal assembly is heparan sulphate dependent we produced mutants based on this model with reduced heparan sulphate binding activity. Their association (k_a) and dissociation (k_d) rate constants of the molecular interactions between polymeric heparin and fibrillin-1 protein fragments and their dissociation constants (K_D), were investigated by surface plasmon resonance using BIAcore 3000.

Wild-type PF9 bound to the heparin saccharide dp24 with a high affinity (K_D 13±1.0 nM; χ^2 5.2±2.0), and with similar kinetics to our previous study (Cain et al., 2005). BIAcore analysis of the R1691A and R1692A single mutants, and the R1691A/R1692A double mutant proved difficult, and the kinetics could not be reliably measured. However, semi-quantitative analysis of the data indicated that these mutants had markedly disrupted heparin binding, indicating that the R1691/R1692 site is important for binding heparin. The effects of two further Arg-to-Ala mutants in the second possible binding site (R1697A and R1752A) had little effect on heparin binding. The double mutant R1697A/R1752A had a K_D of 17±2.1 nM (χ^2 4.5±1.1), and very similar kinetics to wild-type PF9, indicating that these mutations do not disrupt heparin binding to PF9 and thus that this site is unlikely to bind heparin. Interestingly, R1691 and R1692, which are close to the start of the TB5 motif, are fully conserved in mammalian fibrillin-1, and are conserved as RK in fibrillin-2, fibrillin-3 and puffer fish, emphasising their functional importance. The overall percentage amino acid identity of TB5-cbEGF25 in human and bovine fibrillin-1 is 100% and of PF14 is 98.8%. All available mammalian and fish fibrillin-1 sequences also have the TB4 RGD motif.

The non-heparan sulphate binding PF9 double mutant (R1691/R1692) does not support the formation of focal adhesions and stress fibres

Having identified the heparin-binding site within PF9, we investigated the effects of adding soluble R1691A/R1692A PF9 double mutant on MEF and REF cytoskeletal organisation.

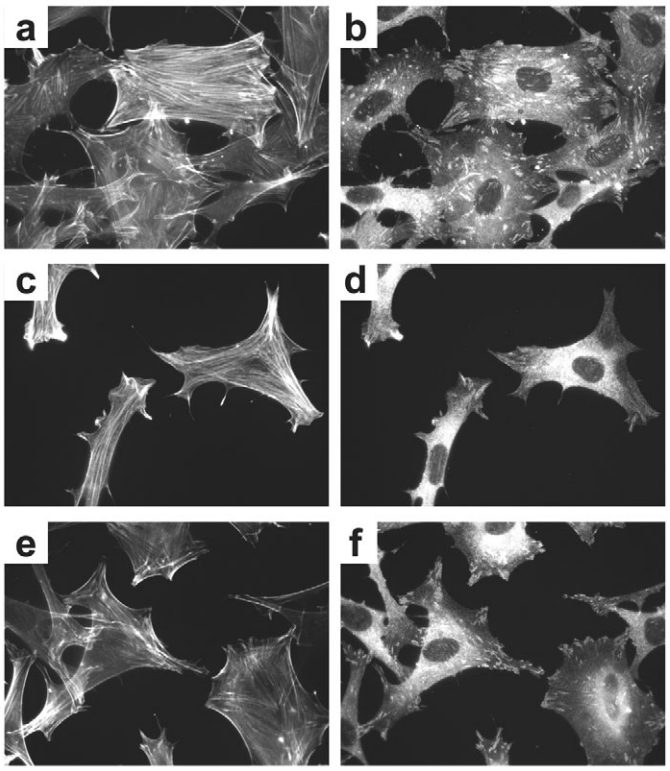

	Vinculin Containing Plaques	Non-Vinculin Containing Plaques	Total Number of Cells	Vinculin Containing Plaques (%)
FN	54	8	62	87
PF8	8	66	74	11
PF8 + PF10	53	26	79	67

Fig. 4. (A) Immunofluorescence images of actin (a,c,e) and vinculin (b,d,f) in REFs adherent to 10 μg/ml fibronectin (a,b) or PF8 (c,d). In e,f, 1 μg/ml PF10 was added in solution for 30 minutes before fixation. (B) The table shows quantification of the number of cells on FN, PF8, or PF8+PF10 fragments that express vinculin-containing and non-vinculin-containing focal plaques (±s.d.).

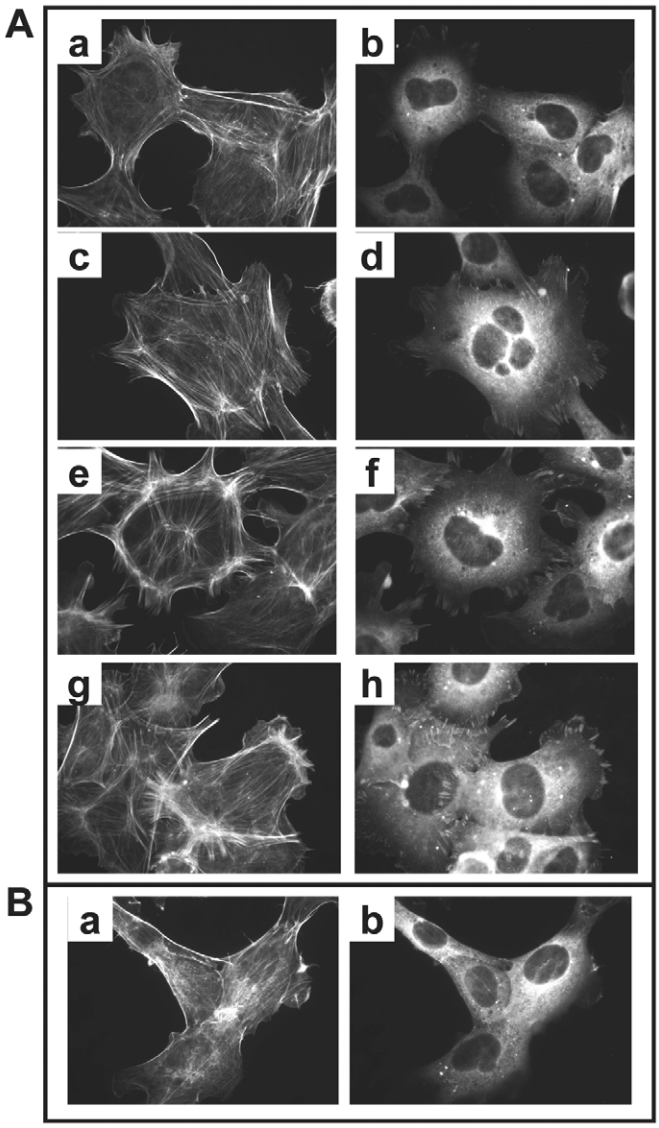

Fig. 5. (A) Immunofluorescence images of actin (a,c,e,g) and vinculin (b,d,f,h) in MEFs adherent to 10 μg/ml PF8 (a-h) for 2 hours. 10 μg/ml of the heparan sulphate binding fragments of fibrillin-1 PF9 (c,d), PF10 (e,f) and PF11 (g,h) were added in solution for 30 minutes before fixing. Quantification revealed that 9% of cells on PF8, 57% of cells on PF8 + soluble PF10, 38% of cells on PF8 + soluble PF9 and 11% of cells on PF8 + soluble mutant PF9 were positive for vinculin and focal adhesions.
(B) Immunofluorescence images of actin (a) and vinculin (b) in MEFs adherent to PF8 in the presence of soluble 10 μg/ml heparan sulphate binding mutant R1691A/R1692A PF9.

MEF cells adherent to PF8 (Fig. 5B), or REF cells adherent to 110FN (Fig. 6C) supplemented with this mutant PF9 failed to induce any focal adhesions or stress fibres, unlike cells supplemented with wild-type PF9. The result confirms that binding to this heparan sulphate binding site is responsible for stimulating focal adhesion and stress fibres.

Discussion

The complexity of cell adhesion interactions with ECM molecules is increasingly apparent. In the case of fibronectin, it is well documented that adhesion to α5β1 integrins requires an upstream synergy motif, and that concurrent engagement of a downstream heparan sulphate binding site by syndecan-4 enhances focal adhesion formation (Woods et al., 2000). We previously showed that fibrillin-1 supports RGD-dependent cell adhesion through α5β1 and αvβ3 integrins (Bax et al., 2003). In this study, we have further characterised HDF adhesion to fibrillin-1, focussing on the molecular requirements for α5β1 adhesion. We also explored the possibility that a downstream heparan sulphate binding site might influence spreading and focal adhesion formation. Our data show that fibrillin-1 adhesion to α5β1 and migration on α5β1 is strongly enhanced by an upstream cbEGF-like domain array. In addition, we have mapped a downstream heparan sulphate binding site and shown that it stimulates focal adhesion formation. The study also highlights the importance of comparing larger fragments when defining adhesion characteristics, rather than RGD peptides or single domains, which may have inappropriate conformations.

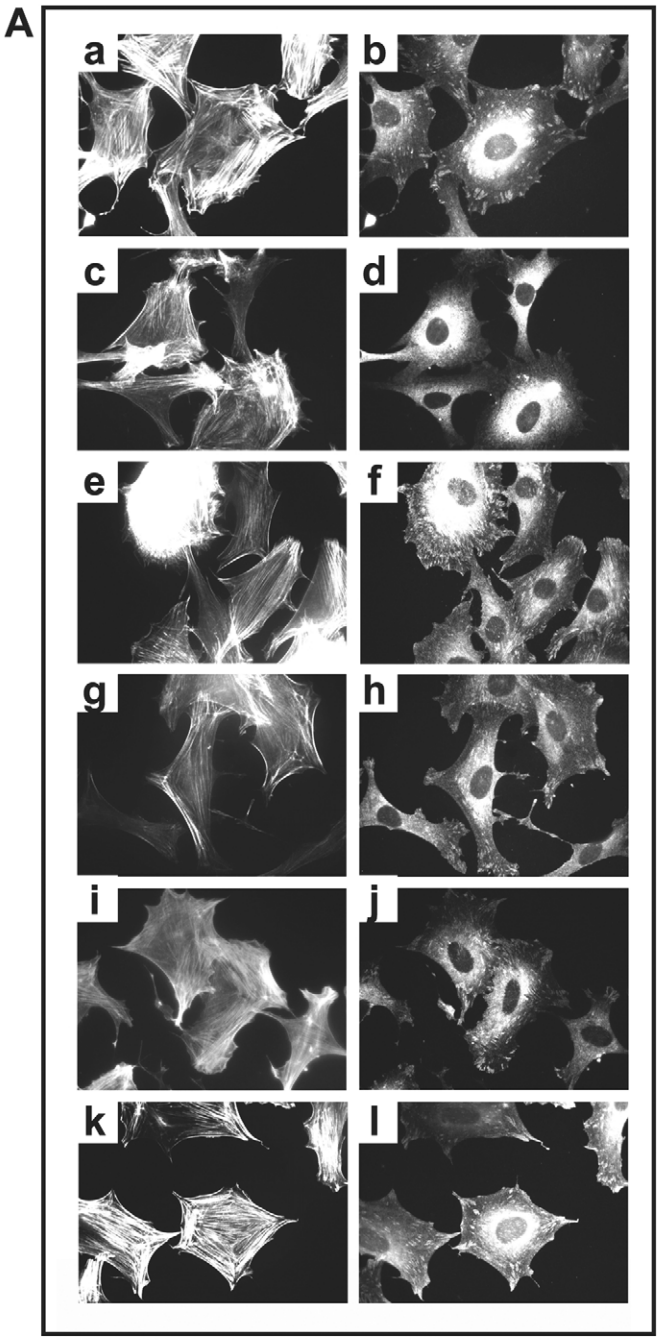

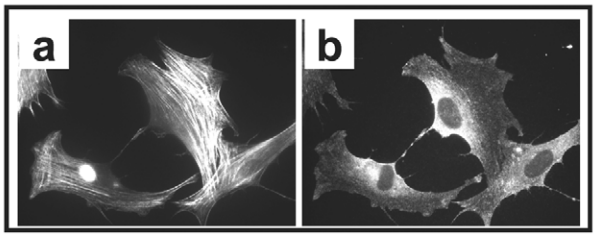

	Vinculin Containing Plaques	Non-Vinculin Containing Plaques	Total Number of Cells	Vinculin Containing Plaques (%)
FN	68	15	83	82
110	14	56	70	20
110 +PF9	52	37	89	58
110 + PF9 - RDG	49	43	92	53
110 + PF10	71	40	111	64
110 + HepII	79	18	97	81
110 + PF9 - R1691A/ R1692A	15	79	94	16

Fig. 6. (A) Immunofluorescence images of actin (a,c,e,g,i,k) and vinculin (b,d,f,h,j,l) in REFs adherent to 10 μg/ml fibronectin (a,c) or to a fragment containing the central cell binding region of fibronectin (110-FN) (c-l) for 2 hours. The heparan sulphate binding fibrillin-1 fragments (10 μg/ml) PF9 (e,f), an RGD-to-RDG mutant PF9 (g,h), PF10 (i,j), or the heparan sulphate binding region of fibronectin (HepII) (k,l) were added in solution for 30 minutes before fixing. (B) The table shows quantification of the number of cells on FN, 110, or 110+fibrillin-1 fragments that express vinculin-containing and non-vinculin-containing focal plaques (±s.d.). (C) Immunofluorescence of actin (a) and vinculin (b) in REFs adherent to 10 μg/ml of 110-fibronectin for 2 hours. Soluble 10 μg/ml heparan sulphate binding mutant R1691A/R1692APF9 was added for 30 minutes before fixing.

PF8, which has seven upstream cbEGF-like domains, supports strong HDF adhesion mainly through α5β1 integrin, unlike PF11 or PF9, neither of which have any upstream cbEGF-like domains and support only weak cell adhesion mainly through αvβ3 integrin (Bax et al., 2003). Thus, there is a major requirement for the presence of upstream cbEGF-like domains for strong adhesion. PF14, which has only four upstream cbEGF-like domains, supported slightly lower adhesion than PF8, perhaps because of long-range conformation effects of the additional three upstream domains. cbEGF 22 is required for RGD-dependent TB4 adhesion to αvβ3 integrin (Lee et al., 2004), but here we have shown, in the context of the PF14 fragment, that substitution of cbEGF-like domain 20 for 22 does not alter HDF adhesion and spreading. Since the requirement for cbEGF 22 can be fulfilled by cbEGF 20, no specific sequence within cbEGF 22 is required. However, the presence of the cbEGF-like domain preceding TB4 may influence the orientation and availability of the RGD motif. The removal of cbEGF-like domains 21 and 22 dramatically reduced adhesion, so there is a requirement for four upstream domains and possibly specifically for cbEGF 21. Substitution of cbEGF 19-22 with cbEGF 3-6 grossly inhibited adhesion, so the specific cbEGFs 19-22, or cbEGFs 19-20-21-20, are needed for strong α5β1-mediated adhesion. Since the fibronectin synergy sequence PHSRN (Redick et al., 2000) is not present in PF14, this specific and essential upstream domain array either contains a novel synergy motif or provides a very specific structural context for the RGD motif. Surprisingly, knock-in of cbEGF 19 or cbEGFs 20-21 into the cbEGF 3-6PF14 construct both rescued strong adhesion, so both knock-in fragments must confer crucial structural effects. The presence of these sugars on cbEGF 19 and 21 may alter conformation, thereby influencing cell adhesion to PF14. All domain swap fragments had correct cbEGF domain junctions and secondary structures.

Having found that cbEGFs 19 and 20-21 induce strong cell adhesion, we compared the fibronectin PHSRN-RGD distance (~3-4 nm) with the distances of cbEGFs 19-21 from the fibrillin-1 RGD motif. Our recent small angle X-ray scattering analysis of recombinant human fibrillin-1 fragments in

solution, expressed in human cells and N-glycosylated, in solution revealed a non-linear conformation of cbEGF-like domain arrays, and provided information on the solution structures of PF8, PF9 and PF10 (Baldock et al., 2006). PF8 has a U-shaped structure with a curvature in the array between cbEGFs 19 and 20, which may be influenced by the N-linked sugars on cbEGFs 19 and 21. Based on the SAXS data, simulations of PF8 typically give the distance from the RGD to the preceding cbEGF-like domains as RGD – cbEGF 22 (4 nm), RGD – cbEGF 21 (6 nm), RGD – cbEGF 20 (8 nm) and RGD – cbEGF 19 (9 nm). There is some degree of curvature bringing cbEGF 19 back towards the RGD motif, which is why the spacing is only slightly greater than between cbEGF 20 and the RGD. To achieve a distance similar to PHSRN-RGD, there would have to be a complete folding back between cbEGF 20-21, but there is no evidence of this from the SAXS data. Therefore, cbEGFs 19-21, which are highly conserved in fibrillins, must exert specific conformational constraints on RGD presentation. This is the first demonstration of such critical long-range effects on $\alpha_5\beta_1$ mediated RGD-dependent adhesion.

A recent report implicated αvβ6, an epithelial integrin, in supporting cell adhesion and focal adhesion formation on fibrillin-1 (Jovanović et al., 2007). This integrin is not generally expressed by HDF. In our studies, in the absence of upstream domains (PF9, Fig. 3C), the very limited HDF adhesion to fibrillin-1 is accounted for by α5β1 and αvβ3 integrins. Jovanović et al. (Jovanović et al., 2007) also concluded that α5β1 is a low-affinity fibrillin-1 receptor, which may reflect their use of short recombinant fragments that lacked upstream cbEGFs 19-21.

Having previously identified a fibrillin-1 heparan sulphate binding site in TB5, which is just three domains downstream of the RGD-containing TB4 (Cain et al., 2005) and is present in PF9, PF10 and PF11, we investigated whether this site could influence cell spreading and focal adhesion formation, using rodent fibroblasts (Humphries et al., 2005; Dovas et al., 2006). We found that all three of these fragments stimulated focal adhesion formation when cells were on PF8, which engages with $\alpha_5\beta_1$ integrin. Following this result and drawing on our previous 3D model of two putative heparin binding sites within TB5 (Cain et al., 2005), we mapped the binding site using mutant fragments and BIAcore analysis to one of these sites (R1691A and R1692A) and then used a double mutant (R1691A/R1692A PF9) to confirm that this conserved site did indeed account for heparan-sulphate-mediated stimulation of focal adhesions. Heparan sulphate occurs at the cell surface in the form of syndecan receptors (Couchman, 2003) and fibronectin is well known to interact with syndecan-4 in conjunction with α5β1, thereby stimulating focal adhesion. Preliminary studies in our laboratory, using syndecan 4-null cells, suggest a similar role for syndecan-4 in fibrillin-1 mediated adhesion (see supplementary material Fig. S1).

It is striking that both fibrillin-1 and fibronectin have an α5β1 integrin-ligating RGD motif and adjacent syndecan heparan sulphate binding site. Since fibrillin-1 and fibronectin have no primary structural homology, these functional motifs might be dictated by cell surface receptors. Fibrillin is an ancient, evolutionarily preserved protein that has been identified at molecular and microfibril levels in primitive Cnidaria such as jellyfish and sea cucumber, which are evolutionarily separated from man by ~1000 million years (Reber-Muller et al., 1995; Thurmond and Trotter, 1996). Such adhesion 'cassettes' which profoundly influence cell behaviour, may be a general feature of ECM molecules that engage α5β1 integrin.

Materials and Methods

Reagents

Inhibitory rat anti-human α5 integrin subunit antibody mAb 16, was a gift from Ken Yamada (NIH, Bethesda, USA). The activating mouse anti-human β1 integrin monoclonal antibody TS2/16 was a gift from Francesco Sanchez-Madrid (Centro de Investigaciones Biológicas, CSIC, Madrid, Spain). A monoclonal anti-αvβ3 integrin antibody (LM609) was obtained from Chemicon International (Temecula, CA). A mouse anti-human paxillin monoclonal antibody and a mouse anti-human α-actinin antibody were obtained from Chemicon. Mouse anti-human vinculin ascities fluid and normal mouse IgG were obtained from Sigma Chemical Company (Dorset, UK). FITC-conjugated anti-mouse secondary antibody was obtained from DAKO (Glostrup, Denmark). Rhodamine-conjugated phalloidin was obtained from Invitrogen (Paisley, UK). A recombinant 50 kDa fibronectin fragment comprising type III repeats 6-10 was produced, as previously described (Mould et al., 1998).

Site-directed mutagenesis PCR primers were synthesised using pfu Turbo polymerase obtained from Stratagene. All other restriction enzymes and ligases were obtained from New England Biosciences. DH5α *E. coli* for bacterial transformations were obtained from Invitrogen (Paisley, UK). All DNA purifications were performed using Qiagen (Crawley, UK) DNA mini or maxi kits.

HDFs were obtained from Cascade Biologics (Portland, OR) and were used up to passage 6. REFs were established in the Couchman laboratory. Wild-type MEFs were available from the Humphries laboratory.

Recombinant fibrillin-1 protein fragments for cell adhesion assays

Recombinant fibrillin-1 protein fragments PF8 and PF11 were expressed and purified as previously described (Bax et al., 2003; Rock et al., 2004). Recombinant fibrillin-1 fragment PF14 (amino acids 1362-1688) was expressed and purified using the modified mammalian episomal expression system pCEP-pu/AC7, which incorporated an N-terminal His_6 tag (Fig. 1A). Following expression in 293-EBNA cells, PF14 was purified from serum-free cell medium using nickel affinity chromatography, as previously described (Bax et al., 2003). PF14 had the correct molecular mass as determined by SDS-PAGE (Fig. 1B), size fractionation on a Superdex 75 column and small angle X-ray scattering (not shown) (Baldock et al., 2006) and circular dichroism (250 μl of 1 mg/ml of each fragment, read at 190-260 nm; six repeats).

Site-directed mutagenesis of Asp1541 to alanine was used to generate the RGD-RGA PF14 mutant. To generate domain swap PF14 protein fragments, site-directed mutagenesis was used to introduce a conservative *Acc*I site at the cbEGF 20-21 domain boundary. This site, and a naturally occurring *Acc*I site at the cbEGF 22/TB4 boundary, allowed the removal of cbEGFs 21 and 22, thereby fusing cbEGF 20 in-frame onto TB4 (designated 19-20PF14). Using mutagenesis to introduce a conservative *Bsr*GI site at the cbEGFs 21-22 boundary, and a naturally occurring *Bsr*GI site at the cbEGF 19-20 boundary, cbEGFs 20 and 21 were inserted in-frame between cbEGF 19 and 20 of the 19-20PF14 construct. This fusion resulted in an in-frame replacement of cbEGF 22 with cbEGF 20, designated 19-20-21-20PF14. The 3-4-5-6 PF14 mutant in which cbEGFs 19-22 were replaced in-frame with cbEGFs 3-6 was constructed by PCR of cbEGFs 3-6, using a mutagenic primer to incorporate a conservative *Acc*I site at the cbEGF 6/TB2 domain boundary. Using this site, and the naturally occurring *Acc*I site at the cbEGF 22/TB4 boundary of PF14, cbEGFs 3-6 were spliced in-frame onto TB4 in place of cbEGFs 19-22. This construct was designated 3-4-5-6PF14.

A knock-in mutant in which cbEGF 3 of 3-4-5-6PF14 was replaced with cbEGF 19 was constructed by introduction of a conservative *Bsr*GI site at the cbEGF 3-4 boundary of 3-4-5-6PF14. Using a *Bam*HI site within the cloning site of the pCEP-pu/AC7 expression vector, and a naturally occurring *Bsr*GI site at the cbEGFs 19-20 boundary of wild-type (WT) PF14, cbEGF 3 was removed from 3-4-5-6PF14 and replaced in-frame with cbEGF 19. This construct was designated 19-4-5-6PF14.

A knock-in mutant in which cbEGFs 4 and 5 of 3-4-5-6 PF14 were replaced with cbEGF-like domains 20 and 21 was constructed using a naturally occurring *Bsr*GI site at the cbEGF-like domains 19-20 boundary, and a conservative *Bsr*GI site introduced at the cbEGF-like 21-22 boundary of the 19-20-21-20PF14 mutant. Conservative *Bsr*GI sites introduced at the cbEGF-like domains 3-4 and 5-6 boundaries of 3-4-5-6PF14 allowed for removal of cbEGFs 4 and 5 and replacement with cbEGFs 20 and 21 from the 19-20-21-20PF14 mutant. This construct was designated 3-20-21-6PF14.

The following primers were used for site-directed mutagenesis to introduce the mutations into WT PF14 that were required to generate the domain swap and knock-in mutants: WT PF14: Forward, 5′-GTCGACCTGGACGAATGTTCCAATGG-3′ and Reverse, 5′-GGATCCTACATGCAATTATTTCCCCC-3′; RGA mutant of

PF14: Forward, 5′-CGACCTCGAGGAGCCAATGGAGATACAGCC-3′ and Reverse, 5′-GGCTGTATCTCCATTGGCTCCTCGAGGTCG-3′; cbEGF 20-21 *Acc*I Site: Forward, 5′-GGGAAAGCCTGTGTAGACATTGATGAGTGCTCC-3′ and Reverse, 5′-GGAGCACTCATCAATGTCTACACAGGCTTTCCC-3′; cbEGF 21-22 *Bsr*GI Site: Forward, 5′-GGCGGGAACTGTACAGATGTGAATGAATGC-3′ and Reverse, 5′-GCATTCATTCACATCTGTACAGTTCCCGCC-3′; 3-4-5-6PF14: Forward, 5′-GTCGACGTTGATGAATGTGAGAAAAACCCC-3′ and Reverse, 5′-CCGCATGTGTGTGTCTACACACACACGGCC-3′; cbEGF 3-4 *Bsr*GI Site: Forward, 5′-CGCGGACAGAATGTACAGACATTGATG-3′ and Reverse, 5′-CATCAATGTCTGTACATTCTGTCCGCG-3′; cbEGF 5-6 *Bsr*GI Site: Forward, 5′-CAGATGGACGTTATTGTACAGACATTAACG-3′ and Reverse, 5′-CGTTAATGTCTGTACAATAACGTCCATCTG-3′.

All the recombinant PF14 domain swap and knock-in protein fragments were N-glycosylated, as determined by PNGaseF treatment, and were the correct molecular mass, as judged by SDS PAGE in the absence or presence of 10 mM dithiothreitol (Fig. 1B,C).

Recombinant fibrillin-1 protein fragments for heparin binding assays

Wild-type human fibrillin-1 fragment PF9 (residues 1528-2166) was expressed using the 293-EBNA expression system, as described (Bax et al., 2003). Single mutants R1691A, R1692A, R1697A and R1752A, and a double mutant R1691A/R1692A, were derived from wild-type PF9 by site-directed mutagenesis. The double mutant R1697A/R1752A was derived from the R1697A mutant by site-directed mutagenesis, using the R1752A mutagenic primers. All mutant constructs were fully sequenced before subcloning into the pCEP-pu/AC7 vector, which had been modified to incorporate an N-terminal His_6 tag following the BM-40 signal peptide (Bax et al., 2003; Cain et al., 2005; Baldock et al., 2006). All constructs were expressed in the 293-EBNA mammalian episomal expression system and purified from culture medium using nickel affinity purification. The following primers were used for site-directed mutagenesis to introduce mutations into fibrillin-1 fragment PF9 and identify the heparin-binding site by testing our previous model (Cain et al., 2005). R1691A Forward, 5′-GCATGGATATGGCAAGA-AGTTTGTCGTACAG-3′ and Reverse, 5′-CTGTAGCACAAACTTCTTGC-CATATCCATGC-3′; R1692A Forward, 5′-GCATGGATATGAGAGCAAGTT-TGTGCTACAG-3′ and Reverse, 5′-CTGTAGCACAAACTTGCTCTCATAT-CCATGC-3′; R1697A Forward, 5′-GAAGTTTGTGCTACGCAAACTACTAT-GCTG-3′ and Reverse, 5′-CAGCATAGTAGTTTGCGTAGCACAAACTTC-3′); R1752A Forward, 5′-CTCTGTGGAAGTCAAGCGCCAGGCTTTGTCATCG-3′ and Reverse, 5′-CGATGACAAAGCCTGGCGCTTGACTTCCACAGAG-3′); R1961A/R1692A Forward, 5′-GCATGGATATGGCAGCAAGTTTGTGCTACT-3′ and Reverse, 5′-CTGTAGCACAAACTTGCTGCCATATCCATG-3′.

All mutagenic fragments had the correct molecular mass as determined by SDS-PAGE in the presence and absence of 10 mM dithiothreitol and size fractionation on a Superdex 75 column. All were N-glycosylated, as seen by electrophoretic shifts in the presence of PNGase F.

Circular dichroism

The secondary structural contents of WT PF14 and domain-swap mutant fragments and WT PF9 and mutant fragments, were investigated by circular dichroism (CD) (Table 1). Far UV (190-260 nm) CD spectra were recorded on a Jasco J-810 spectropolarimeter at 190-260 nm, using 250 μl of a 0.5 mg/ml solution of each fragment, with six repeats. Measurements were taken every 0.2 nm in a 0.05 cm path length cell. Samples were measured directly from the light scattering experiments in buffer supplemented with 1 mM $CaCl_2$, to ensure that the samples were monomeric (Mellody et al., 2006). Spectra were corrected for buffer absorbance, and represented an average of ten scans. Spectra were recorded in millidegrees and converted to mean residue ellipticities using concentrations estimated by absorbance profiles at 280 nm. Deconvolution of the CD raw data for each protein fragment was performed using CDSSTR software programme (Sreerama and Woody, 2000) available on online server dichroweb (Whitmore and Wallace, 2004) (http://www.cryst.bbk.ac.uk/cdweb/html/home.html). All the PF14 domain-swap fragments and the PF9 mutant fragments had similar secondary structures to the wild-type fragments and as predicted for their domain structures.

Homology alignments

Amino acid sequences of cbEGF 19-22 and TB4, and of TB5 and cbEGF 25, respectively, from fibrillins of human, bovine, pig, mouse, rat and fish (*Tetraodon nigroviridis*), were aligned using Clustal W (1.83) (Higgins et al., 1994).

Cell attachment and spreading assays

Cell attachment assays were performed as previously reported (Bax et al., 2003). Each recombinant fibrillin-1 fragment, or fibronectin, was diluted in PBS containing 1 mM Ca^{2+} (Mellody et al., 2006) at protein-coating concentrations from 0-20 μg/ml, and absorbed onto wells of a 96-well microtitre plate (Costar, Acton, MD) for 1 hour at 20°C. Unbound ligand was aspirated, and non-specific binding was blocked with 10 mg/ml heat-denatured (85°C for 10 minutes) bovine serum albumin (BSA) (Sigma), at 20°C for 1 hour. Cell suspensions were prepared by incubating cell layers with trypsin-EDTA at 37°C for 4 minutes, followed by neutralisation with an equal volume of medium containing 10% FCS. The cell suspensions were centrifuged at 800 ***g*** for 3 minutes, and the cell pellets were resuspended in 5 ml of warm DMEM/HEPES. Cell numbers were counted and adjusted to 5×10^5 cells/ml. The cell suspensions were then incubated for 20 minutes at 37°C with the lid off in a 5% CO_2 incubator. The BSA blocking solution was aspirated from the ligand-coated wells, which were then washed with 200 μl PBS. To determine cell attachment to adhesion ligands, 100 μl cells (mixed prior to use by gentle pipetting) were added to the appropriate wells. Alternatively, to examine the effects of inhibitory antibodies, 50 μl 2× concentration of antibody was added to the wells followed by 50 μl cells at 1×10^6, to give final antibody protein concentrations of 10 μg/ml. Data were statistically analysed using unpaired Student's *t*-tests (GraphPad Prism 2.0). Error bars represent the s.d. of the three experiments. Results were statistically significant when $P<0.05$ (*$P<0.05$, **$P<0.001$, ***$P<0.0001$).

To determine % attachment, known numbers of cells were added to uncoated, unblocked wells. The microtitre plates were incubated for 20 minutes at 37°C in a 5% CO_2 incubator with the lid off. Known cell number control wells were fixed by addition of 10 μl of 50% glutaraldehyde. Non-adherent cells were removed from the other wells by aspiration, and attached wells were fixed with the addition of 100 μl of 5% glutaraldehyde. Microtitre plates were incubated at room temperature for 20 minutes and washed three times with 200 μl dH_2O. Cells were stained with 100 μl of 0.1% (w/v) crystal violet in 0.2 M MES pH 5.0, and incubated at room temperature for 1 hour. The crystal violet was aspirated, and excess stain was removed by four washes with 400 μl dH_2O. The dye was solubilised in 100 μl of 10% (v/v) acetic acid, and the absorbance measured at 570 nm using a Dionex MRX II microtitre plate reader. Background crystal violet staining readings were subtracted from all experimental and known percentage cell results. The data from the 'known cell number' wells were plotted using Microsoft Excel and the slope of the line used to express data as percentage cell attachment. In all experiments, triplicate wells were prepared.

To determine cell spreading, the wells of microtitre plates were ligand coated and BSA blocked as for cell attachment assays. The cells were trypsinised, quenched and counted as before, then adjusted to 2×10^5 cells/ml. 100 μl aliquots of cells were added to ligand-coated and control uncoated, BSA-blocked wells. The plate was incubated for 40 minutes at 37°C in a 5% CO_2 incubator with the lid off. The cells were immediately fixed with the addition of 10 μl of 37% (w/v) formaldehyde directly to the well for 20 minutes. The formaldehyde was aspirated, and the wells filled with PBS before layering a glass coverslip onto the plate. The level of cell spreading was determined by phase-contrast microscopy. Cells were spread when 'phase-dark' with visible nuclei, but unspread when rounded and 'phase-bright'.

BIAcore 3000 kinetic analysis of heparin interactions with wild-type and mutant PF9

Kinetic binding studies of heparin, using saccharide dp24, with fibrillin-1 were conducted using a BIAcore biosensor and surface plasmon resonance, as previously reported (Cain et al., 2005) (BIAcore 3000, BIAcore AB, Sweden). Biotinylated heparin dp24 fragments were immobilised onto commercially prepared SA sensor chips, which have pre-immobilised streptavidin, to allow biotin capture. Using a heparin concentration of 1 μM, typically 150-200 response units (RU) of biotinylated heparin samples were immobilised, which was at a saturation level. Samples were applied to the sensor chip surface in 0.1 M NaOAc pH 5.5. All subsequent binding experiments were performed in 10 mM HEPES pH 7.4, 0.1 M NaCl, 1 mM $CaCl_2$ and 0.005% surfactant P20 (designated HBS-Ca). Protein fragments were injected at concentrations ranging from 1-20 μg/ml at a flow rate of 12 μl/minute. Samples were injected for 12 minutes, dissociated for 10 minutes, regenerated for 2× 1 minute using 5 mM NaOH, 1 M NaCl, and then stabilised for 10 minutes before the next injection. After subtraction of each response value from the blank cell, association and dissociation rate constants were determined by global data analysis. All curves were fitted using 1:1 Langmuir association/dissociation model (BIAevaluation 4.1, BIAcore AB), which was previously shown to be appropriate for the PF9-heparin interaction (Cain et al., 2005).

Table 1. The secondary structural contents of WT and domain swap PF14 fragments determined by CD

PF 14	Alpha helix	Beta strand	Turns	Unordered
WT	4	40	22	34
3-4-5-6	4	40	23	33
3-20-21-6	4	44	21	31
19-4-5-6	4	42	20	34

Deconvolution of the raw data for each fragment was performed using CDSSTR software programme (Sreerama and Woody, 2000), which is available on the online server dichroweb (Whitmore and Wallace, 2004) (http://www.cryst.bbk.ac.uk/cdweb/html/home.html). The PF14 fragments all had similar secondary structures as predicted by their domain structures.

Immunofluorescence microscopy

HDFs, REFs (Dovas et al., 2006) and wild-type and syndecan-4 null MEFs (Humphries et al., 2005) were analysed. Ethanol-cleaned glass coverslips were coated in a 24-well plate as outlined in cell attachment and spreading assays. Briefly the cover slips were coated using 500 μl ligand at room temperature for 2 hours. Non-specific cell binding to the glass was blocked by incubation with 1 ml of 10 mg/ml BSA for 1 hour. Cells were prepared as in attachment and spreading assays to a density of 5×10^5 cell/ml and 500 μl of cells were added per well for 2 hours at 37°C in 5% CO_2. In some experiments, adherent cells were treated with 1-10 μg/ml heparan sulfate binding fragments for 30 minutes. Cells were fixed with the addition of formaldehyde to 3% (w/v) for 20 minutes, then quenched with 500 μl 0.1 M glycine. The cells were permeabilised with 500 μl of 0.5% (v/v) Triton X-100 for 4 minutes, then blocked with 1 ml of 3% filter-sterilised BSA (BSA block) for 1 hour at room. After blocking, the coverslips were incubated in 500 μl of 10 μg/ml primary antibody diluted in BSA block for 1 hour at room temperature, then in 500 μl of 1 μg/ml FITC-labelled secondary antibody with 1:1000 (v/v) rhodamine-conjugated phalloidin diluted in BSA block for 30 minutes at room temperature. The coverslips were mounted in a drop of Vecta shield including DAPI (Vector Labs, Burlingame, USA) on glass slides and sealed with nail varnish before viewing using an Olympus microscope fitted with a UV lamp and appropriate filters. Basic image acquisition and analysis was performed using MetaVue. Advanced image analysis was performed using Adobe Photoshop v6.0. Focal adhesions were quantified as previously published (Dovas et al., 2006).

Migration

Wells of a 24-well plate were coated in protein and blocked as described for immunofluorescence. HDFs were prepared as for cell attachment and spreading assays and diluted to 1×10^5 cells/ml. 1 ml of cells was added per well and incubated on the 37°C heated stage of a Leica AS MDW microscope with a 5% CO_2 jacket for 1 hour. After incubation, *x*,*y* and *z* co-ordinates were set up in triplicate for each well for an in-focus photo. Photos were taken every 10 minutes for a 16-hour period. Distance measurements were made using imageJ, and the distance travelled was calculated from the change in *x* and *y* co-ordinates of the cell position using Pythagoras' calculation.

This work was funded by the UK Centre for Tissue Engineering (MRC, BBSRC and EPSRC) and the European Commission (LSHM-CT-2005-018960). Y.M. and J.R.C. were supported by Wellcome Trust Programme Grant 065940.

References

Alexopoulou, A. N., Multhaupt, H. A. and Couchman, J. R. (2007). Syndecans in wound healing, inflammation and vascular biology. *Int. J. Biochem. Cell Biol.* **39**, 505-528.

Baldock, C., Siegler, V., Bax, D. V., Cain, S. A., Mellody, K. T., Marson, A., Haston, J. L., Berry, R., Wang, M. C., Grossmann, J. G. et al. (2006). Nanostructure of fibrillin-1 reveals compact conformation of EGF arrays and mechanism for extensibility. *Proc. Natl. Acad. Sci. USA* **103,** 11922-11927.

Bax, D. V., Bernard, S. E., Lomas, A., Morgan, A., Shuttleworth, C. A., Humphries, M. J. and Kielty, C. M. (2003). Cell adhesion to fibrillin-1 molecules and microfibrils is mediated by α5β1 and αvβ3 integrins. *J. Biol. Chem.* **278,** 34605-34616.

Cain, S. A., Baldock, C., Gallagher, J., Morgan, A., Bax, D. V., Weiss, A. S., Shuttleworth, C. A. and Kielty, C. M. (2005). Fibrillin-1 interactions with heparin. Implications for microfibril and elastic fiber assembly. *J. Biol. Chem.* **280,** 30526-30537.

Couchman, J. R. (2003). Syndecans: proteoglycan regulators of cell-surface microdomains? *Nat. Rev. Mol. Cell Biol.* **4**, 926-937.

Dovas, A., Yoneda, A. and Couchman, J. R. (2006). PKCalpha-dependent activation of RhoA by syndecan-4 during focal adhesion formation. *J. Cell Sci.* **119**, 2837-2846.

Higgins, D. G. (1994). CLUSTAL V: multiple alignment of DNA and protein sequences. *Methods Mol. Biol.* **25**, 307-318.

Humphries, M. J., Mostafavi-Pour, Z., Morgan, M. R., Deakin, N. O., Messent, A. J. and Bass, M. D. (2005). Integrin-syndecan cooperation governs the assembly of signalling complexes during cell spreading. *Novartis Found. Symp.* **269**, 178-188.

Jovanović, J., Takagi, J., Choulier, L., Abrescia, N. G., Stuart, D. I., van der Merwe, P. A., Mardon, H. J. and Handford, P. A. (2007). alpha Vbeta 6 is a novel receptor for human fibrillin-1: comparative studies of molecular determinants underlying integrin-RGD affinity and specificity. *J. Biol. Chem.* **282**, 6743-6751.

Kielty, C. M. (2006). Elastic fibres in health and disease. *Expert Rev. Mol. Med.* **8**, 1-23.

Kielty, C. M., Sherratt, M. J., Marson, A. and Baldock, C. (2005). Fibrillin microfibrils. *Adv. Protein Chem.* **70**, 405-436.

Lack, J., O'Leary, J. M., Knott, V., Yuan, X., Rifkin, D. B., Handford, P. A. and Downing, A. K. (2003). Solution structure of the third TB domain from LTBP1 provides insight into assembly of the large latent complex that sequesters latent TGF-beta. *J. Mol. Biol.* **334**, 281-291.

Lee, S. S., Knott, V., Jovanović, J., Harlos, K., Grimes, J. M., Choulier, L., Mardon, H. J., Stuart, D. I. and Handford, P. A. (2004). Structure of the integrin binding fragment from fibrillin-1 gives new insights into microfibril organization. *Structure* **12**, 717-729.

Mellody, K. T., Freeman, L. J., Baldock, C., Jowitt, T. A., Siegler, V., Raynal, B. D., Cain, S. A., Wess, T. J., Shuttleworth, C. A. and Kielty, C. M. (2006). Marfan syndrome-causing mutations in fibrillin-1 result in gross morphological alterations and highlight the structural importance of the second hybrid domain. *J. Biol. Chem.* **281**, 31854-31862.

Mould, A. P., Garratt, A. N., Puzon-McLaughlin, W., Takada, Y. and Humphries, M. J. (1998). Regulation of integrin function: evidence that bivalent-cation-induced conformational changes lead to the unmasking of ligand-binding sites within integrin alpha5 beta1. *Biochem. J.* **331**, 821-828.

Pereira, L., D'Alessio, M., Ramirez, F., Lynch, J. R., Sykes, B., Pangilinan, T. and Bonadio, J. (1993). Genomic organization of the sequence coding for fibrillin, the defective gene product in Marfan syndrome. *Hum. Mol. Genet.* **2**, 961-968.

Pfaff, M., Reinhardt, D. P., Sakai, L. Y. and Timpl, R. (1996). Cell adhesion and integrin binding to recombinant human fibrillin-1. *FEBS Lett.* **384**, 247-250.

Reber-Muller, S., Spissinger, T., Schuchert, P., Spring, J. and Schmid, V. (1995). An extracellular matrix protein of jellyfish homologous to mammalian fibrillins forms different fibrils depending on the life stage of the animal. *Dev. Biol.* **169**, 662-672.

Redick, S. D., Settles, D. L., Briscoe, G. and Erickson, H. P. (2000). Defining fibronectin's cell adhesion synergy site by site-directed mutagenesis. *J. Cell Biol.* **149**, 521-527.

Ritty, T. M., Broekelmann, T. J., Werneck, C. C. and Mecham, R. P. (2003). Fibrillin-1 and –2 contain heparin-binding sites important for matrix deposition and that support cell attachment. *Biochem. J.* **375**, 425-432.

Rock, M. J., Cain, S. A., Freeman, L. J., Morgan, A., Mellody, K., Marson, A., Mellody, K. C., Shuttleworth, C. A., Weiss, A. S. and Kielty, C. M. (2004). Molecular basis of elastic fiber formation. *J. Biol. Chem.* **279**, 23748-23758.

Sakamoto, H., Broekelmann, T., Cheresh, D. A., Ramirez, F., Rosenbloom, J. and Mecham, R. P. (1996). Cell-type specific recognition of RGD- and non-RGD-containing cell binding domains in fibrillin-1. *J. Biol. Chem.* **271**, 4916-4922.

Sreerama, N. and Woody, R. W. (2000). Estimation of protein secondary structure from circular dichroism spectra: comparison of CONTIN, SELCON, and CDSSTR methods with an expanded reference set. *Anal. Biochem.* **287**, 252-260.

Thurmond, F. and Trotter, J. (1996). Morphology and biomechanics of the microfibrillar network of sea cucumber dermis. *J. Exp. Biol.* **199**, 1817-1828.

Tiedemann, K., Batge, B., Muller, P. K. and Reinhardt, D. P. (2001). Interactions of fibrillin-1 with heparin/heparan sulfate, implications for microfibrillar assembly. *J. Biol. Chem.* **276**, 36035-36042.

Tiedemann, K., Sasaki, T., Gustafsson, E., Gohring, W., Batge, B., Notbohm, H., Timpl, R., Wedel, T., Schlotzer-Schrehardt, U. and Reinhardt, D. P. (2005). Microfibrils at basement membrane zones interact with perlecan via fibrillin-1. *J. Biol. Chem.* **280**, 11404-11412.

Whitmore, L. and Wallace, B. A. (2004). DICHROWEB, an online server for protein secondary structure analyses from circular dichroism spectroscopic data. *Nucleic Acids Res.* **32**(Web Server issue), W668-W673.

Woods, A., Longley, R. L., Tumova, S. and Couchman, J. R. (2000). Syndecan-4 binding to the high affinity heparin-binding domain of fibronectin drives focal adhesion formation in fibroblasts. *Arch. Biochem. Biophys.* **374**, 66-72.

Yuan, X., Downing, A. K., Knott, V. and Handford, P. A. (1997). Solution structure of the transforming growth factor β-binding protein-like module, a domain associated with matrix fibrils. *EMBO J.* **16**, 6659-6666.

Zhang, H., Apfelroth, S. D., Hu, W., Davis, E. C., Sanguineti, C., Bonadio, J., Mecham, R. P. and Ramirez, F. (1994). Structure and expression of fibrillin-2, a novel microfibrillar component preferentially located in elastic matrices. *J. Cell Biol.* **124**, 855-863.